



## “Crypton 1.0”: Accurate cyclic voltammetry forecasting of activated carbon electrode with machine learning

Adisa Jarubenjaluk, Pannapha Kullattanapratep, Apinporn Pornpipattanasiri,  
Kulpavee Jitapunkul\*, Pawin Iamprasertkun\*

School of Bio-Chemical Engineering and Technology, Sirindhorn International Institute of Technology, Thammasat University, Pathum Thani 12120, Thailand

### ARTICLE INFO

**Keywords:**  
Crypton  
Machine learning  
Energy storage  
Artificial neural network  
Cyclic voltammetry  
Activated carbon  
LiTFSI

### ABSTRACT

Cyclic voltammetry (CV) is a technique for determining the electrochemical properties of the electrode, and electrolyte in electrochemical systems. However, it is sensitive to various feature, and the correlation between them is not fully explained hitherto. An artificial neural network (ANN) was employed to create a CVs prediction for further explain the electrochemical properties in “water-in-salt” electrolyte e.g., scan rate, electrolyte concentration, and potential window. The electrochemical assistant software based on the developed model are then present (namely “Crypton 1.0” beta version). The designed network architecture consists of two hidden layers with fixed number of neurons in the latter to reduce the calculation burden for loop training. Five-fold cross validation and single loop training with a variation of hidden neurons in the first hidden layer from 1 to 20 neurons were applied to generalize the prediction. The training was performed in batches corresponding to positive scan, negative scan, and full cycle scan to achieve comprehensive models. The final predictions are the product of averaged models with coefficient of determination ( $R^2$ ) over 0.98 for each scanning characteristic. Interestingly, the prediction for wide potential windows showed superior accuracy comparable with the CV from experimental measurement. In addition, the electrochemical stability window has been investigated, and found to be increased along with the electrolyte concentration explaining the concepts of using “water-in-salt” electrolyte. This work covers the understanding of electrochemistry and the model development via ANN for software development. Therefore, our work could be an alternative approach to reduce the experimental burden in the future development of electrochemical applications.

### Abbreviations

ANN	Artificial neural network
CV	Cyclic voltammetry
ESW	Electrochemical stability window
LiTFSI	Lithium bis(trifluoromethanesulfonyl)imide
MIMO	Multiple-input-multiple-output
$R^2$	Coefficient of determination
RMSE	Root-mean-square-error

### Introduction

Energy storage devices with high efficiency and affordable electrode are under continuous development due to the sustainable development policy (UN-SDG7). Supercapacitors are one of the promising devices that can fulfill the energy storage system due to its high-power density and

tunable energy density [1]. Supercapacitors can provide ultra-fast charge and discharge rate with a considerably long life cycle [2]. Activated carbon is the sole commercialized carbonaceous material that has been utilized as the electrode in electric double layer capacitor (EDLC). Since commercial activated carbon typically possesses a high cycle stability, high porosity, and large surface area, while maintaining low market price due to high throughput production with physical and chemical procedures [3]. Lithium bis(trifluoromethanesulfonyl)imide (LiTFSI) is a favorable “water-in-salt” electrolyte due to its broad electrochemical stability window (up to 3.0 V) [4,5] that can extend beyond the thermodynamic limit of water splitting [4,6]. However, each of electrochemical system exhibits its own electrochemical characteristic (refer to CV profiles) [7]; hence, the experimental work are required for clarify its own electrochemical behavior. A ton of electrochemical result have been done in the past decade [8–10]. Therefore, to produce a practical outcome of the future electrochemical research, the cyclic

\* Corresponding authors.

E-mail addresses: [kulpavee.aj@siit.tu.ac.th](mailto:kulpavee.aj@siit.tu.ac.th) (K. Jitapunkul), [pawin@siit.tu.ac.th](mailto:pawin@siit.tu.ac.th) (P. Iamprasertkun).

voltammetry forecasting is then present in this work. The commercial activated carbon (YEC-8A) and LiTFSI were selected as model electrode and electrolyte for this study, respectively. Since the introduction of cyclic voltammetry (CV) over decades ago, this electroanalytical measurement has been routinely used to provide thermodynamics of reaction, electron transfer kinetics [11,12], and electrochemical performance for energy storage [13] and conversion [14]. Consequently, owing to its ability to provide cyclic trace between current of working electrode versus applied voltage, the capacitive performance of electrode can be determined from CV profiles [15,16]. To our knowledge, CV measurement is sensitive to experimental parameters that could affect the reaction and mass transport mechanisms. Thus, the repetition under the same conditions may result in a slightly deviated CV profile (see Fig. S1), possibly due to equipment or human errors. From this reason, we are convinced that machine learning can be a futuristic approach to generate generalized CV profile based on gathered experimental measurements. The application of machine learning has substantially grown in the past decades to improve prediction accuracy and computational efficiency in multidisciplinary scientific research [17–20]. Due to the fact that machine learning can provide insight on underlying relationship between system's parameters, its predictive ability tends to be improved with optimized training strategies [20]. Literatures have reported the usage of machine learning, especially artificial neural networks (ANN) can predict the electrochemical properties of supercapacitors [21,22]. Dongale et al. has proposed a shallow ANN model that can accurately predict CV profile of MnO<sub>2</sub> thin film electrode based on measured current density and potential sweep from −1.0 to 1.0 V with scan rate of 10 mV s<sup>−1</sup>. Their model has been trained with Levenberg–Marquart backpropagation algorithm and sigmoid transfer function has been applied to the single hidden layers with 3 hidden neurons [23]. Jitapunkul et al. has reported the usage of shallow ANN coupled with Levenberg–Marquardt backpropagation can precisely predict the CV profile of size-dependent graphene based on graphene flake size and multiple scan rates with coefficient of determination ( $R^2$ ) of 0.98. The double loop training with variation of hidden neurons has been adopted to expand the generalization of model. The optimum number of hidden neurons for final model is found to be 7 neurons which is larger than number of inputs, but, smaller than total number of training samples [24]. In addition, a few literatures have reported the usage of ANN to predict capacitance of promising materials for supercapacitors' electrode based on several electrochemical features such as specific surface area, or amount of heteroatom-doping etc. [19,25–28]. Herein, we proposed the predictive ANN model to generate CV profile of commercial activated carbon (demonstrated with YEC-8A) electrode with LiTFSI electrolyte (concentration ranging from “salt-in-water” to “water-in-salt”). The model training has been performed based on our in-house measurement with wide range of electrolyte concentrations, scan rates, and potential windows. To cover the full range of practical experimental parameters which eventually lead to practical prediction. Apart from the prediction ability of the model, the electrochemical stability windows, and underlying relationship between essential electrochemical properties versus the CV profiles have been discussed. Moreover, we have developed the CV prediction/calculation software (“**Crypton 1.0**” beta version-inspire from “Cyclic voltammetry prediction by trained and optimized network”) for assisting the researcher on their experimental work. Thus, this work should introduce the extensive usage of machine learning interlinked with the electrochemical context to gain better understanding of carbon-based electrodes, which facilitate the development of energy storage devices.

## Methodology

### Cyclic voltammograms of activated carbon electrode

Three electrode configurations were implemented for CV measurement, the electrodes used in the experiment are reference, counter, and

working electrode. The reference electrode and counter electrode are Ag/AgCl (ItalSens, glass coated, 80 mm long, 4 mm in diameter) and Pt wire (ItalSens, PTFE / Kel-F [PCTFE] coated, 70 mm long, 0.5 mm Pt diameter), respectively. The working electrode is glassy carbon (IS-3 MM.GC.WE.1, 0.0707 cm<sup>2</sup>) coated with 2 µL of AC paste (total mass loading of 0.178 mg). For the activated carbon paste, it was a combination of an 8:1:1 mass ratio of YEC-8A activated carbon (Fuzhou Yihuan Carbon Co. Ltd; surface area ≥ 1800 m<sup>2</sup> g<sup>−1</sup>; particle size ~10 µm; ash 0.26%, iron content < 0.005%, moisture < 5%), PVDF (Sigma Aldrich), and carbon blacks (Alpha Aesar with 99% purity). The powder slurry is then blended with NMP (Loba Chemie with 98% purity) in grams to milliliters of 1:9 and stirred for 6 h to form AC paste. The glassy carbon is polished by the procedure employed by Elgrishi et al., (2018) [29]. After coating the circular active area, the electrode is then dried for 30 min at 60 °C in the vacuum oven. LiTFSI (Sigma Aldrich with 99.95% purity) electrolytes were prepared at concentrations of 1, 5, 10, and 20 m (from “salt-in-water” to “water-in-salt”) where the conductivity of the given electrolytes are 20.01, 50.03, 31.7825, and 10.425 mS cm<sup>−1</sup> and viscosities are 1.25, 2.82, 7.25, and 45.62 mm<sup>2</sup> s<sup>−1</sup>, respectively. The cyclic voltammetry response of activated carbon electrode in LiTFSI electrolytes were recorded using potentiostat (Autolab PGSTAT302N). Scanning conditions were manipulated via NOVA software (version 2.0). For each LiTFSI concentration, CV curves were scanned at scan rates of 10, 25, 50, 75, and 100 mV s<sup>−1</sup> while potential windows are sweeping from 0.1 (with potential step of 0.1 V) to their positive and negative maximum branch for individual concentration. Generally, the reported maximum potential window accomplished is around 3.0 V for 21 m LiTFSI “water-in-salt” electrolyte in the case of stainless steel electrodes which is a nonactive material [4]. Therefore, all the concentrations are attempted to scan up to 3.0 V to examine curves pattern slightly beyond decomposition potentials. It is noted that the 1 and 5 m LiTFSI can be scanned to an overall of 2.8 V (−1.4 to 1.4 V) while 10 and 20 m can be extended to 3.0 V (−1.5 to 1.5 V). Otherwise, the curves were not connected properly due to the noise generated from electrochemical reaction e.g., hydrogen, and oxygen evolution [7]. A single run at a specified condition provided 3 CV curves: negative, positive, and full window cyclically sweeping from 0.0 V to the negative potential limit, the positive potential limit, and the full range including positive and negative limit, respectively. Noted that all CVs reported in this work are comparative to an Ag/AgCl reference electrode.

### Pre-processing of cyclic voltammetry data through segmented data reduction

The CV measurements were cumulatively collected as 870 datasets and categorized into three groups according to scan characteristics as follows: (i) negative scan (NEG), (ii) positive scan (POS), and (iii) full cycle scan (FULL). Each group will be trained by separated ANN models to reduce the relation complexity and avoid the confusion of algorithm, which may lead to inaccurate prediction. Each group contains 290 CV profiles corresponding to variated range of electrolyte concentrations, potential windows, and scan rates as explained in previous section (see Table S1). However, due to limitation in measurement, the different potential sweeping, and scan rates have caused variation in number of data points of CV profiles. Unfortunately, neural network training requires identical data entries for both input and output of all training samples. Therefore, the pre-processing of data is necessary for reformatting the raw CV profiles to have identical number of data points which will later be used as output for neural network training. Thus, the segmented data reduction was applied to adjust the data entry of each CV to be 100 points for current response data and 100 points for corresponding potential data to relieve the training load (see supporting information under section “Segmented data reduction” for detail procedure).

### Design and training of artificial neural network

According to the CV measurements, there are three major parameters that significantly affect the shape of cyclic profile: (i) electrolyte concentration, (ii) potential sweeping window, and (iii) scan rate. Thus, the inputs of neural network training were selected to be the numerical value of LiTFSI concentration in a unit of molal (m), absolute value of potential sweeping limit in a unit of volts (V), and numerical value of scan rate in a unit of millivolts per seconds ( $\text{mV s}^{-1}$ ). On the other hand, outputs of the network were the processed cyclic sweeping data entries in form of current responses and the corresponding potential values, which can be visualized as CV profiles. Consequently, three identical multiple-input-multiple-output (MIMO) networks were established for training the datasets from separated scan characteristic (NEG, POS, and FULL). In general, the neural network architecture consists of three main components which are input layer, hidden layer(s), and output layer. However, the number of hidden layers and the hidden neurons usually be optimized via trial-and-error approach [30]. Several recommendations are made to assist the determination of hidden neurons that will

optimize the model performance. One suggestion stated that maximum number of neurons in all hidden layer should equal to the number of samples [31]. Therefore, the determination of network architecture in this study has been performed via trial-and-error in combination with single loop training through hidden neurons variation. Here, we proposed the ANN model design for training of data from separated scan characteristics in MATLAB2022b (license number 40904941, Thammasat University) as illustrated in Fig. 1a. K-fold cross validation was concurrently executed to extend the generalization of training (Fig. 1b, see supporting information for more detail). Thus, the variation of hidden neurons was only performed in the first hidden layer to reduce the computational burden. This single-loop variation should sufficiently introduce generality of training through random initial weight and bias. The hyperbolic tangent sigmoid transfer function ("tansig") normalized radial basis transfer function ("radbasn"), and linear transfer function ("purelin") have been utilized in hidden layer 1, hidden layer 2, and output layer, respectively. The resilient backpropagation algorithm was used for training to avoid the effect of persisting small weight and bias magnitude with sigmoid transfer function [32]. The final prediction is

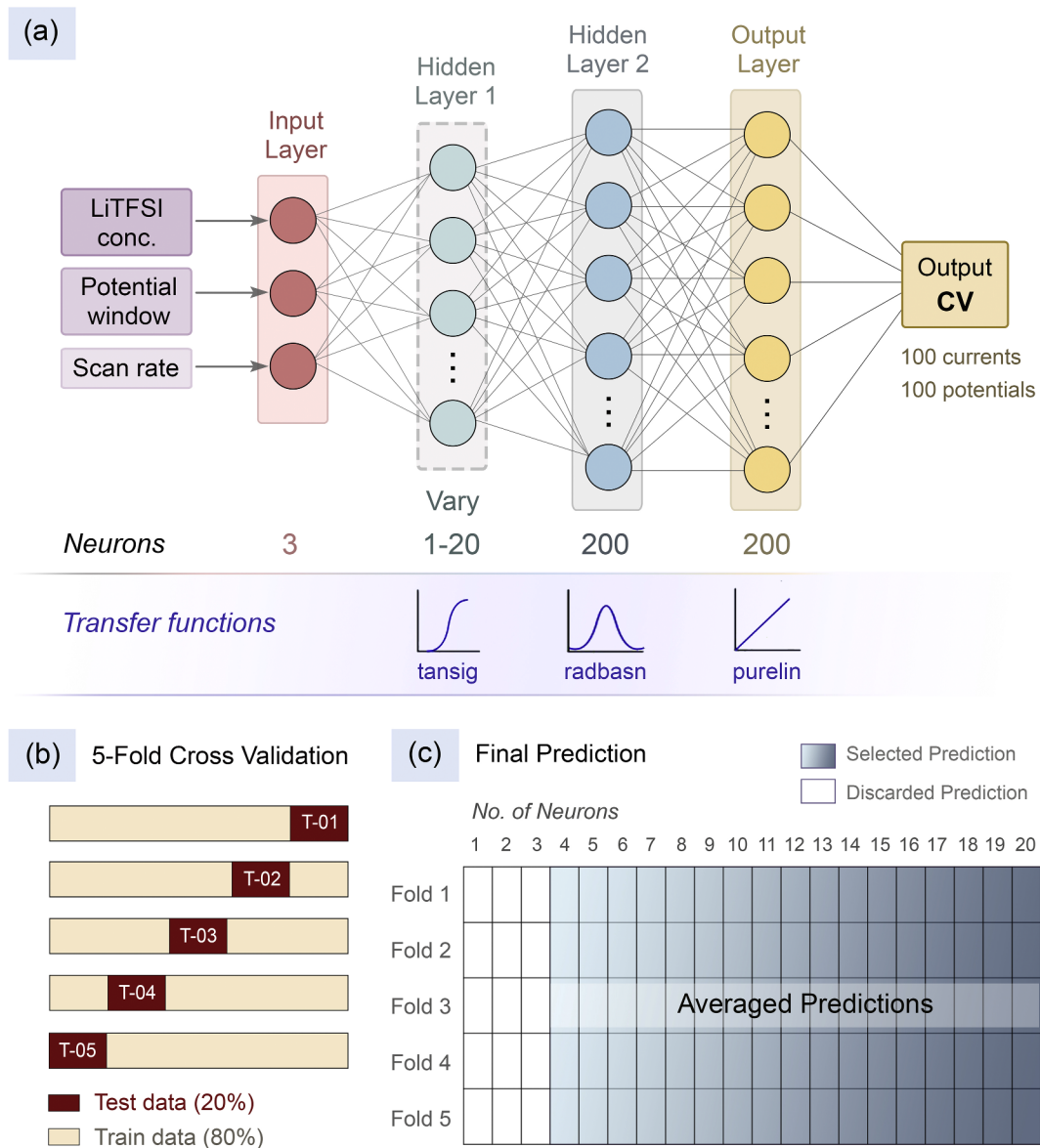


**Fig. 1.** Schematic diagram of the ANN design, training procedure, and generation of final prediction. (a) The ANN architecture with number of neurons and transfer functions for each layer. (b) K-Fold cross validation framework for data division into test and train sets with label "T-01", "T-02", "T-03", "T-04", and "T-05" refer to different test set for each fold. (c) Final prediction schematic based on averaging predictions from selected network models.

the product of averaged models with high prediction efficiency determined by coefficient of determination ( $R^2$ ), which calculated using Eq. S1, across K-fold cross validation as shown in Fig. 1c. Nevertheless, the overfitted model will be the major cause of poor prediction. Thus, early stopping is additionally implemented in the training where 10% of the training data is carved out known as the validation set. This regularization will stop the training once the validation error is increasing for 6 consecutive iterations and then returned the weight and bias at minimum validation error. In addition, 10 datasets have been randomly extracted from each scan characteristic group prior to the training for ultimate evaluation of the trained networks.

## Result and discussion

### Electrochemical stability window

The term electrochemical stability window (ESW) is an important indicator that describes the stable working potential limit (range) of electrolytes [33]. ESW plays a role by ensuring that electrolyte retains inertness before the oxidation and reduction reactions occur [13]. Those side reactions cause electrolyte decomposition, which influences the selection of electrodes in energy storage devices, thereby the potential outputs and the cell's energy density [33,34]. It is necessary to grasp the significance of investigating the operated potential range for an electrode and electrolyte pair so that the cell can perform in safe regions avoiding the gas evolution [33,35]. Systematic quantification of ESW for activated carbon/electrolyte was established by Xu et.al (2001) [36]. The literature suggested that the scan rate of 5 to 10 mV s<sup>-1</sup> is basically

low enough for utilizing the active area of activated carbon materials (porosity equal to or less than M30 activated carbon (Osaka Gas, Inc.)). Thus, the voltammograms were preliminarily examined by observation where the first reaction peak was noticeable. A scan rate at 10 mV s<sup>-1</sup> was selected for each LiTFSI concentration. ESW of YEC-8A activated carbon electrode in various LiTFSI electrolyte concentrations is displayed in the cyclic voltammograms in Fig. 2. Note, the gas evolution including hydrogen, and oxygen evolution were determined via a stability criterion (S-value). The difference between the S-values of two successive points should not exceed 0.005 for a demonstration of stable voltage [33].

Overall, the onset potential of oxygen evolution is shifted to a more positive potential when the electrolyte concentration is increased. For the low concentration of 1 m LiTFSI (considered as traditional aqueous solution), the oxygen evolution onset occurred about 0.8 V vs. Ag/AgCl on the positive potential (see Fig. 2a) while the hydrogen evolution presents at -1.0 V vs. Ag/AgCl. It is obvious that the onset for 5 m LiTFSI is shifted toward 0.9 V on the positive side while keeping the negative onset at ca. -1.0 V (see Fig. 2b). This indicate that the increase of LiTFSI concentration can diminished the oxygen evolution reaction, which is in excellent agreement with previous report [33]. In addition, concentrations at 10 m (Fig. 2c) and 20 m LiTFSI (Fig. 2d), the onset shifted to 1.0 V and 1.2 V on the cathodic side respectively. At 20 m LiTFSI, it is "water-in-salt" due to the fact that both the weight and volume of Li salt surround by the water (as a solvent) in a binary system [4]. On the other hand, hydrogen evolution happens at a potential value of -1.1 V vs. Ag/AgCl on the negative side for all the concentrations. This suggests that the increase of LiTFSI concentration in activated carbon system only

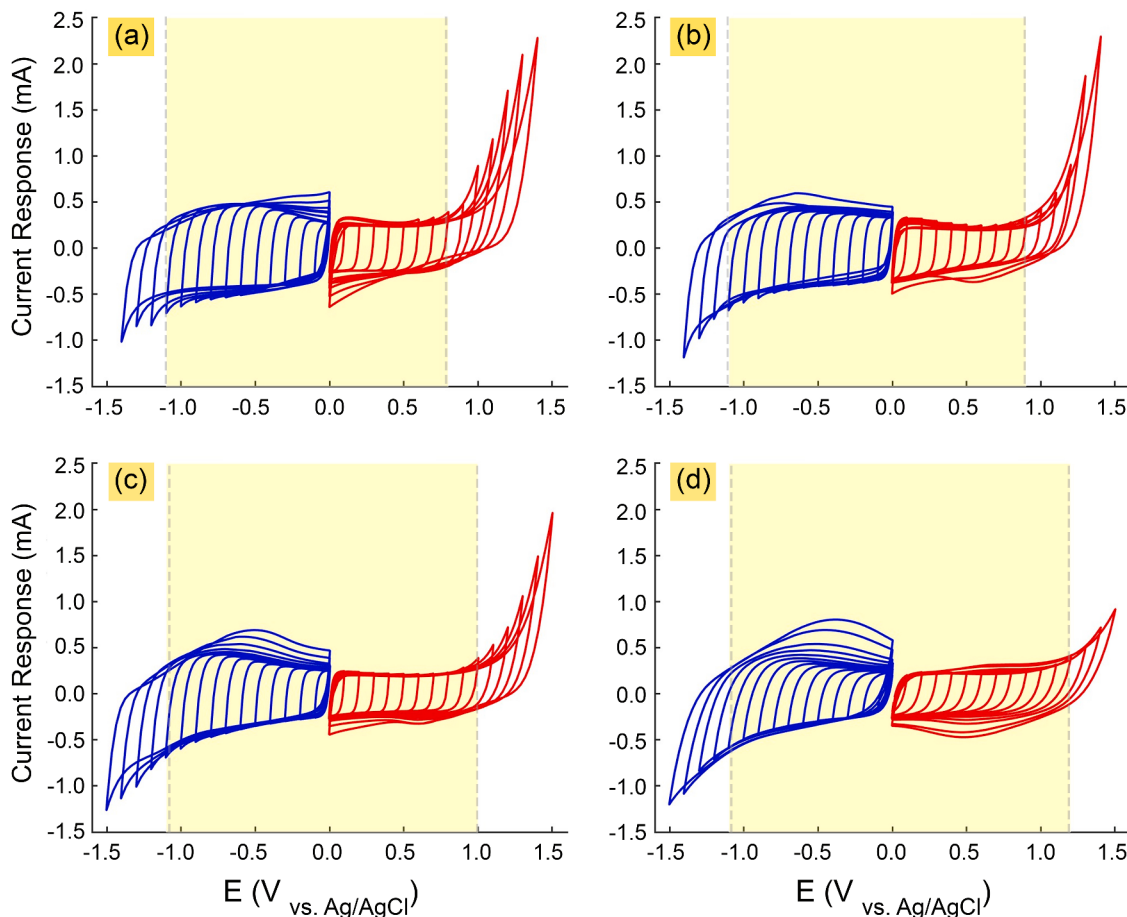


**Fig. 2.** Cyclic voltammograms at scan rate of 10 mV s<sup>-1</sup> with a 0.1 V of potential window interval on activated carbon (grade YEC-8A) electrodes in (a) 1 m LiTFSI, (b) 5 m LiTFSI, (c) 10 m LiTFSI, and (d) 20 m LiTFSI. Blue and red solid cyclic curves represent the negative and positive CVs, respectively. The yellow shade area confined by gray dashed lines depicts the safe region.

suppresses the oxygen evolution reaction while its only slightly affect the onset potential of hydrogen evolution reaction. Determination of practical ESW for 1, 5, 10, and 20 m LiTFSI can be retrieved by subtraction of a positive and negative potential limit yielding 1.9, 2.0, 2.1, 2.3 V, which increases accordingly. This shows that LiTFSI enables the expansion of ESW over the water stability limit (1.23 V) as it delays the oxygen evolution reaction by the formation of the passivation layer [4]. The upward shift of oxygen evolution at positive polarization occurs when LiTFSI concentration increases. Studies elucidate differences in electrolyte concentration will impact the solvation structure in the inner and outer Helmholtz layer at the positive electrode [5]. Mostly, water molecules are present in the inner layer while TFSI anion is in the outer layer for the aqueous LiTFSI. On the other hand, for highly concentrated LiTFSI, the amount of free water is minimized, therefore the amount of TFSI anions is predominant. Thus, a declining amount of water with a denser TFSI anions population is observed when increasing the "water-in-salt" electrolyte concentration [5,37].

#### ANN training performance and optimization

Machine learning has become a prominent tool for a wide range of research studies related to supercapacitors [38]. For instance, optimizing device performance and estimating electrochemical performance such as specific capacitance, galvanostatic charge and discharge (GCD), cyclic voltammetry (CV), and lifespan of supercapacitors [20,23,24,39,40]. However, a concern is that the data used in several studies were collected from different sources. This may introduce the inevitable effects that significantly boost the relation complexity between input and output and affect the accuracy of prediction. From our viewpoint, using data from in-house experiments would be an alternative solution to limit uncontrollable factors that could affect the predictive performance. To the best of our knowledge, the predictive model to generate CV of commercial activated carbon is not reported elsewhere. Consequently, such predictive models are successfully developed here for separated scan characteristics via rigorous training of neural network using in-house experimental measurements. The determination of hidden

layers and corresponding hidden neurons are ambiguous as mentioned in methodology section. We have followed the guideline that the number of hidden neurons should be less than or equal to the number of samples. Because we have split our dataset based on 5-fold cross validation with 20:80 ratio for test and train set, respectively. Thus, we have a total of 224 datasets in the train set and 56 datasets in test set for each scan characteristics (NEG, POS, and FULL). Then, the maximum number of hidden neurons will be set according to the amount of data in train set which is 224. We have started with shallow neural network design. The training of each ANN model was first conducted with hyperbolic tangent sigmoid transfer function through single-loop by variation of hidden neurons from 1 to 20 in single hidden layer. However, the  $R^2$  values of test set are persistently high since the usage of single neuron in the hidden layer (see Fig. S3). This is because we have 3 and 200 data entries for each input and output, respectively. Hence, the shallow network with single hidden neurons should not be sufficient for providing the decent prediction. For this reason, we extended the neural network design to dual hidden layers with different transfer functions (shown in Fig. 1a). Then, performed the single-loop training with variation of hidden neurons from 1 to 20 in the first hidden layer and fixed number of neurons to 200 in the latter one. The  $R^2$  value and root-mean-square-error (RMSE) were used to evaluate the performance of training across 5-fold cross validation as illustrated in Fig. 3. It is very clear that the  $R^2$  values of test set for all scan characteristics groups stabilized at 4 neurons architecture onward as well as the minimization of RMSE. It is suggested that the optimum number of hidden neurons should lie between the number of input and total number of training samples. However, in this study, we are convinced that the determination of single optimum network architecture is not a wise approach. Due to the large number of generated networks from single loop training and 5-fold cross validation for each scan characteristic group. Consequently, we adopted the concept of averaged predictive model instead. It is well-known in general practice that model uncertainty could be reduced by averaging the prediction across several models [41]. Noted, the rigid scientific evidence has not been confirmed hitherto.

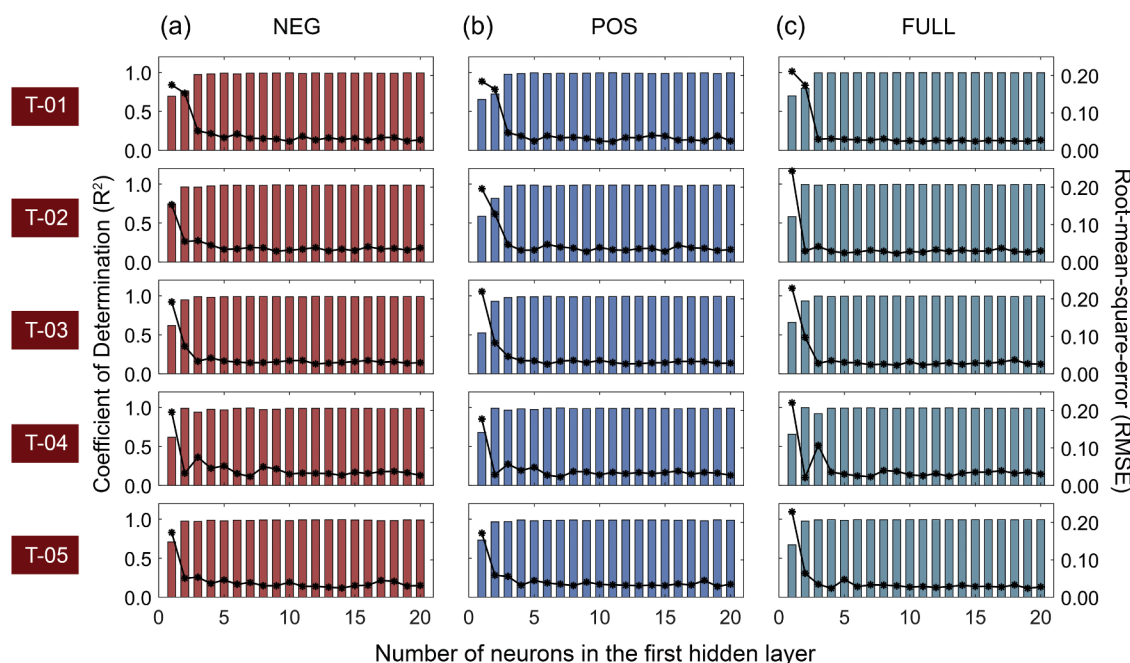


**Fig. 3.** Coefficient of determination ( $R^2$ ) and root-mean-square-error (RMSE) span corresponding to the variation of hidden neurons in the first hidden layer of dual hidden layers network. The bar plots refer to  $R^2$  values with the scale on the left y-axes. The black line plots with asterisk markers refer to RMSE with scale on the right y-axes. (a)  $R^2$  and RMSE from NEG group, (b)  $R^2$  and RMSE from POS group, and (c)  $R^2$  and RMSE from FULL group. Noted that all reported  $R^2$  and RMSE are calculated based on test set in each fold of cross validation which labelled in red boxes located at the left edge of the figure.

### Evaluation of tested CV profiles across 5-fold cross validation

The evaluation of predictive ability can be further performed based on visualization of predicted CV profiles in test set across 5-fold cross validation by comparing with the experimental CVs. Hence, we used the

average prediction, all predicted data from 4 neurons until 20 neurons in the first hidden layer architectures were averaged according to each fold splitting for visualization. It is found that the accuracy of CV prediction for all scan characteristics at small potential window ranging from  $\sim 0.1$  to  $\sim 0.5$  V were substantially lower than the prediction at wider

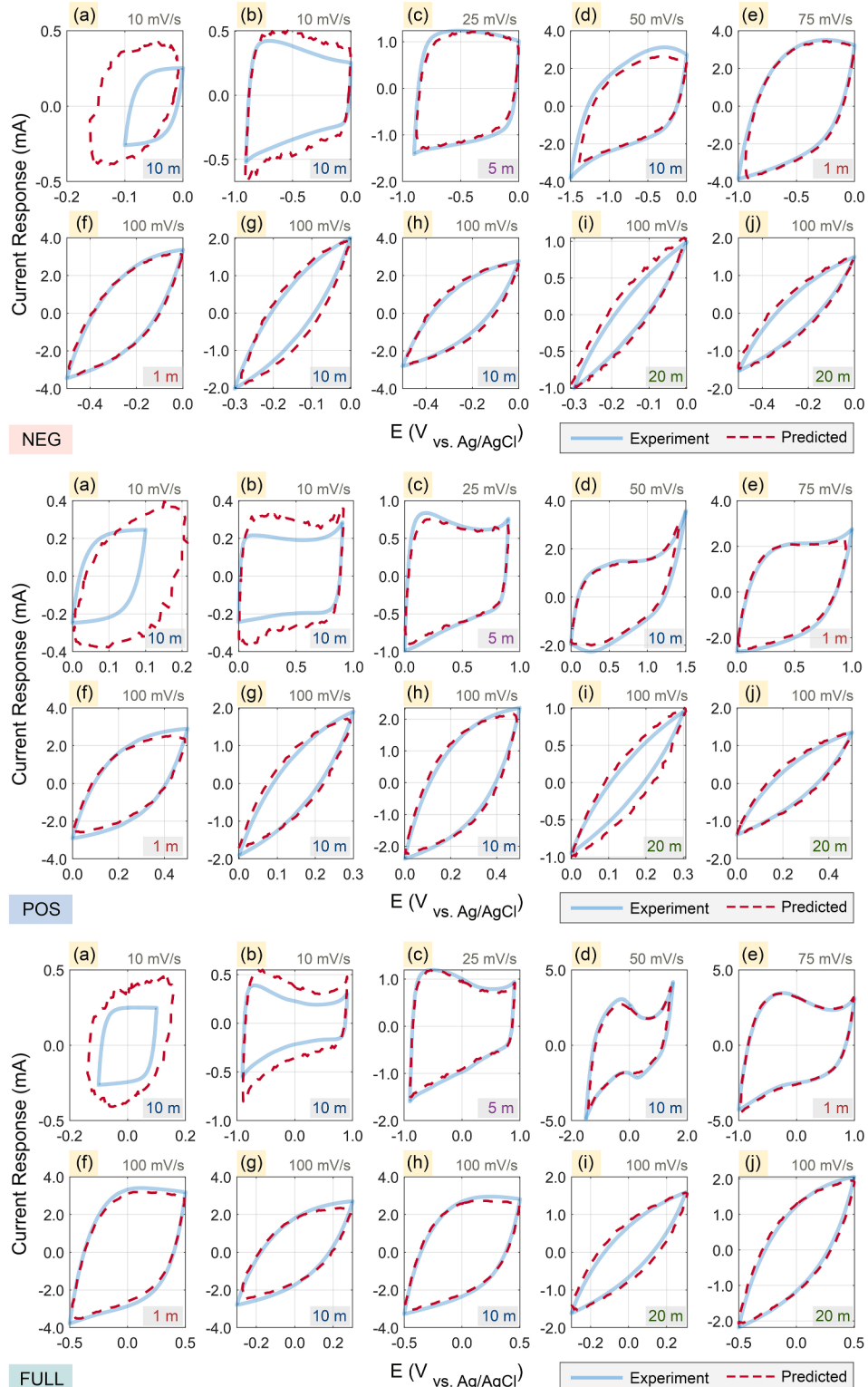


**Fig. 4.** Comparison of predicted CV profiles from unseen datasets with their respective measured values by using the final averaged model from negative, positive, and full sweeping data training (NEG, POS, and FULL). The light blue solid line represents the experimental cyclic profile, and the dashed red line represents the predicted values. The scan rates and LiTFSI concentration were labelled on each subplot (a) to (g) which refers to the alphabet notation specified to each dataset.

potential windows (cf. Fig. S4 to Fig. S18). A precise prediction result obtained from 0.5 to 1.4 V vs. Ag/AgCl. Moreover, the prediction for low scan rate, specifically  $10 \text{ mV s}^{-1}$ , shows a higher degree of deviation from the experimental profile. One speculation for the imprecise CV predictions was possibly due to the different charge storage mechanism of the activated carbon where their store the charge via inner pore instead of outer surface [1]. This may lead to difficulties in establishing the correct correlation between parameters during model training. Therefore, the validity of absolute potential window limit and scan rates that suitable for usage of our predictive model can also be determined accordingly. The valid absolute potential window limit should fall within the range of 0.5 to 1.5 V and the scan rate should be faster than  $10 \text{ mV s}^{-1}$ .

#### *Ultimate prediction of 10 unseen datasets*

The overall predictive behavior across 5-fold cross validation is similar; thus, the final predictions can be performed based on averaging the predictions across 4 to 20 neurons architecture and all folds. We then achieved the 3 separated predictive models for each scan characteristic (NEG, POS, and FULL). Thus, the final evaluation of those models was carried out by predicting the cyclic profiles corresponding to the retained 10 unseen datasets (a to g), which will ensure the model's predictive capabilities as illustrated in Fig. 4. The corresponding  $R^2$  values and RMSE were evaluated for each cyclic profile with respect to the experimental values as listed in Table 1. Evidently, the as-developed model can precisely forecast the electrochemical response of the activated carbon electrode, showing average  $R^2$  of ca. 0.98 and RMSE between 0.0032 and 0.0472.

The outcomes of these predictions demonstrated high  $R^2$  values and low RMSE for the 10 unseen profiles, thereby vaguely verifying the model's overall efficiency. However, the visualization of average prediction revealed that the prediction at either narrow potential window or low scan rate show significant degree of inaccuracy. This once again confirmed that the developed models have limited predictive ability at mention conditions. On the other hand, the prediction for wider potential windows and faster scan rates displayed incredibly high accuracy through visualization and eminent  $R^2$  over 0.99. Therefore, the predictive accuracy of our model can be approximated to be 80% based on 8 accurate profiles out of 10 predictions (see Fig. 4).

#### **Conclusion**

The practical ESW of activated carbon (evaluated at scan rate of  $10 \text{ mV s}^{-1}$ ) is found to be 1.9, 2.0, 2.1, and 2.3 V for 1, 5, 10, and 20 m of LiTFSI, respectively. The enlargement of CV profiles is due to the suppression of the gas evolution reaction. This is because the increase of salt content in solvent ("water") can diminish the free water molecule that solvated around the neat ions. The negative potential limit is found to be constant at 1.1 V for all LiTFSI concentrations while the positive limit is clearly extended corresponding to the higher concentration due to the suppression of oxygen evolution reaction. Apart from the experimental evaluation, the artificial neural network has been successfully trained to forecast the CV profiles of commercial activated carbon electrode, creating "Crypton 1.0" for assisting the electrochemical measurement.

**Table 1**

Coefficient of determination and root-mean squared error of 10 unseen dataset (a to g).

Group	Dataset	(a)	(b)	(c)	(d)	(e)	(f)	(g)	(h)	(i)	(j)
NEG	$R^2$	0.8671	0.9994	0.9992	0.9993	0.9798	0.9897	0.9893	0.9984	0.9992	0.9991
	RMSE	0.0320	0.0074	0.0082	0.0417	0.0462	0.0170	0.0099	0.0062	0.0054	0.0069
POS	$R^2$	0.9216	0.9995	0.9992	0.9998	0.9794	0.9910	0.9932	0.9988	0.9964	0.9989
	RMSE	0.0275	0.0072	0.0107	0.0314	0.0472	0.0160	0.0079	0.0055	0.0071	0.0054
FULL	$R^2$	0.8854	0.9995	0.9975	0.9999	0.9988	0.9897	0.9953	0.9994	0.9974	0.9998
	RMSE	0.0283	0.0088	0.0219	0.0346	0.0148	0.0225	0.0104	0.0061	0.0081	0.0032

Three separated ANN models based on average prediction strategies are proposed herein with 80% accuracy for comprehensive usage. The suitable range of potential window limit was suggested to be  $\sim 0.5$  to 1.5 V as well as the fast scan rates, preferably over  $10 \text{ mV s}^{-1}$ , to increase the predictive performance. Obviously, the rapid charge and discharge rates are necessary for an excellent supercapacitor, which can be achieved with high scan rates. Therefore, our proposed model can effectively be used for forecasting in common practices e.g. capacitance, stable voltage limit, capacitive analysis, which could aid the experimental load for electrochemists, especially supercapacitor field.

#### *Perspectives and outlook*

The scope of information and prediction can be extended to a vast choice of electrode materials and electrochemical system e.g. two to four electrode configurations in a variety of applications (not limit to the energy storage). For the improvement of electrode material, numerous types of activated carbon and carbon-based material can be applied, indicating a variety of surface areas, pore structure, and ash content etc. The formulation of electrode material is also crucial e.g. mixing ratio, additive, and so on. Variety of electrolytes including other high solubility salts and organic solvents, as well as the operating conditions can be further investigated. Extensively, the redox containing system could provide a useful guideline for energy storage system (also refer to pseudocapacitive materials). Eventually, the predicted CVs could potentially be used extensively in determining specific capacitance, capacitive analysis, stable voltage or converting to another type of electrochemical characterization i.e., galvanostatic charge and discharge. Hence, the models will be beneficial by enhancing their functionality to support a wider range of applications.

#### **Funding**

This project is funded by National Research Council of Thailand (NRCT) under contract No. N42A660942.

#### **Author contributions**

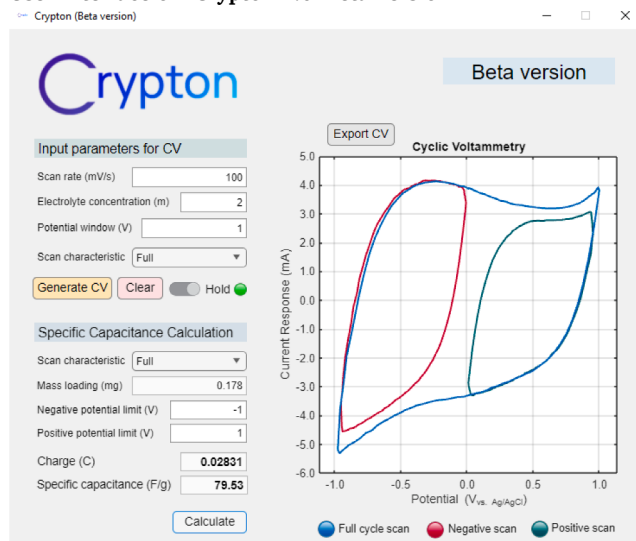
A.J., P.K., and A.P. performed electrochemical measurements, collected the raw data, designed artificial neural network and training, generated illustrations, interpreted results, and wrote manuscripts-first draft. K.J. supervised machine learning procedure, performed data analysis, discussed the result, generated illustrations, and wrote the manuscript. P.I. initiated the project outline, designed the experiment, discussed the result, performed data analysis, funding acquisition, and wrote manuscript including review-editting. The manuscript was written through contributions of all authors. All authors have given approval to the final version of the manuscript.

#### **Supporting information**

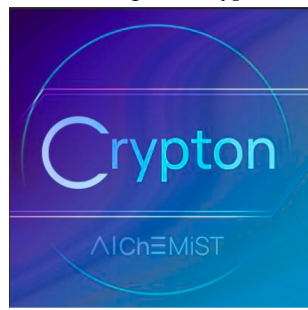
The supporting information has been divided into 5 sections. The first section involves the repetition of CV measurements from experimental aspects. The second section mainly contains additional details related to methodology as follows: the categorization of data, segmented

data reduction procedure in detail, K-fold cross validation, and calculation of coefficient of determination. The third section shows the evaluation of data training with shallow neural network design prior to the finalization of the proposed model. The fourth section contains the plots of predicted CV from test set across 5-Fold cross validation in comparison with experimental CV for three scan characteristics (NEG, POS, and FULL).The fifth section is the detail of provided codes and Crypton application with the link to access our Github repository.The beta version of "Crypton 1.0" and machine learning algorithm (ANN) for cyclic voltammetry forecasting can be download from: <https://github.com/WYAlChEMIST/Crypton> Remarks, for "Crypton 1.0" beta installation please direct to "for\_redistribution" folder and click on the application installer.

### User interface of "Crypton 1.0" beta version



### Interface Logo of "Crypton 1.0"



### Declaration of Competing Interest

The authors declare that they have no known competing financial interests or personal relationships that could have appeared to influence the work reported in this paper.

### Data availability

Data availability: <https://github.com/WYAlChEMIST/Crypton>

### Acknowledgement

This project is funded by National Research Council of Thailand (NRCT) under contract No. N42A660942. Authors acknowledge Thammasat University for providing the license of MATLAB2022b (license number 40904941).

### Supplementary materials

Supplementary material associated with this article can be found, in the online version, at doi:[10.1016/j.cej.2023.100548](https://doi.org/10.1016/j.cej.2023.100548).

### References

- [1] L.L. Zhang, X.S. Zhao, Carbon-based materials as supercapacitor electrodes, *Chem. Soc. Rev.* 38 (9) (2009) 2520–2531.
- [2] Y. Shen, B. Liu, X. Liu, J. Liu, J. Ding, C. Zhong, W. Hu, Water-in-salt electrolyte for safe and high-energy aqueous battery, *Energ. Stor. Mater.* 34 (2021) 461–474.
- [3] I. Gürten II, Scalable activated carbon/graphene based supercapacitors with improved capacitance retention at high current densities, *Turk. J. Chem.* 45 (3) (2021) 927–941.
- [4] L. Suo, O. Borodin, T. Gao, M. Olguin, J. Ho, X. Fan, C. Luo, C. Wang, K. Xu, Water-in-salt" electrolyte enables high-voltage aqueous lithium-ion chemistries, *Science* 350 (6263) (2015) 938–943.
- [5] L. Coustan, G. Shul, D. Bélanger, Electrochemical behavior of platinum, gold and glassy carbon electrodes in water-in-salt electrolyte, *Electrochim. Commun.* 77 (2017) 89–92.
- [6] L. Miao, Z. Song, D. Zhu, L. Li, L. Gan, M. Liu, Recent advances in carbon-based supercapacitors, *Mater. Adv.* 1 (5) (2020) 945–966.
- [7] R.J. Forster, D.A. Walsh, Voltammetry | overview, in: P. Worsfold, A. Townshend, C. Poole (Eds.), *Encyclopedia of Analytical Science* (Second Edition), Elsevier, Oxford, 2005, pp. 181–188.
- [8] R.H. Baughman, A.A. Zakhidov, W.A. de Heer, Carbon Nanotubes—the Route Toward Applications, *Science* 297 (5582) (2002) 787–792.
- [9] J.B. Goodenough, K.S. Park, The Li-Ion Rechargeable Battery: A Perspective, *J. Am. Chem. Soc.* 135 (4) (2013) 1167–1176.
- [10] M. Chhowalla, H.S. Shin, G. Eda, L.J. Li, K.P. Loh, H. Zhang, The chemistry of two-dimensional layered transition metal dichalcogenide nanosheets, *Nat. Chem.* 5 (4) (2013) 263–275.
- [11] J. Heinze, Cyclic Voltammetry—"Electrochemical Spectroscopy". New Analytical Methods (25), *Angew. Chem. Int. Ed. Engl.* 23 (11) (1984) 831–847.
- [12] R.S. Nicholson, I. Shain, Theory of Stationary Electrode Polarography. Single Scan and Cyclic Methods Applied to Reversible, Irreversible, and Kinetic Systems, *Anal. Chem.* 36 (4) (1964) 706–723.
- [13] Y. Gogotsi, R.M. Penner, Energy Storage in Nanomaterials – Capacitive, Pseudocapacitive, or Battery-like? *ACS Nano* 12 (3) (2018) 2081–2083.
- [14] D. McAtee, Z. Ghalmavand, N. McEvoy, A. Harvey, E. O'Malley, G.S. Duesberg, J. N. Coleman, Thickness Dependence and Percolation Scaling of Hydrogen Production Rate in MoS2 Nanosheet and Nanosheet–Carbon Nanotube Composite Catalytic Electrodes, *ACS Nano* 10 (1) (2016) 672–683.
- [15] O. Gharbi, M.T.T. Tran, B. Tribollet, M. Turmine, V. Vivier, Revisiting cyclic voltammetry and electrochemical impedance spectroscopy analysis for capacitance measurements, *Electrochim. Acta* 343 (2020), 136109.
- [16] M. Maher, S. Hassan, K. Shoueir, B. Yousif, M.E.A. Abo-Elsoud, Activated carbon electrode with promising specific capacitance based on potassium bromide redox additive electrolyte for supercapacitor application, *J. Mater. Res. Technol.* 11 (2021) 1232–1244.
- [17] P. Puthongkham, B.J. Venton, Recent advances in fast-scan cyclic voltammetry, *Analyst* 145 (4) (2020) 1087–1102.
- [18] S.N. Dean, L.C. Shriner-Lake, D.A. Stenger, J.S. Erickson, J.P. Golden, S. A. Trammell, Machine Learning Techniques for Chemical Identification Using Cyclic Square Wave Voltammetry, *Sensors* (2019) [Online].
- [19] A. Chenwittayakachon, K. Jitapunkul, B. Nakpalad, P. Worrayotkavit, S. Namuangruk, P. Sirisudomkit, P. Lampraserkun, Machine learning approach to understanding the 'synergistic' pseudocapacitive effects of heteroatom doped graphene, *2D Mater.* 10 (2) (2023), 025003.
- [20] T. Gao, W. Lu, Machine learning toward advanced energy storage devices and systems, *iScience* 24 (1) (2021), 101936.
- [21] S. Zhu, J. Li, L. Ma, C. He, E. Liu, F. He, C. Shi, N. Zhao, Artificial neural network enabled capacitance prediction for carbon-based supercapacitors, *Mater. Lett.* 233 (2018) 294–297.
- [22] M. Zhou, A. Vassallo, J. Wu, Data-Driven Approach to Understanding the In-Operando Performance of Heteroatom-Doped Carbon Electrodes, *ACS Appl. Energy Mater.* 3 (6) (2020) 5993–6000.
- [23] T.D. Dongale, P.R. Jadhav, G.J. Navathe, J.H. Kim, M.M. Karanjkar, P.S. Patil, Development of nano fiber MnO<sub>2</sub> thin film electrode and cyclic voltammetry behavior modeling using artificial neural network for supercapacitor application, *Mater. Sci. Semicond. Process.* 36 (2015) 43–48.
- [24] K. Jitapunkul, A. Chenwittayakachon, P. Lampraserkun, Transition of electrochemical measurement to machine learning in the perspective of two-dimensional materials, *Front. Mater.* 9 (2022).
- [25] A.G. Saad, A. Emad-Eldeen, W.Z. Tawfik, A.G. El-Deen, Data-driven machine learning approach for predicting the capacitance of graphene-based supercapacitor electrodes, *J. Energy Storage* 55 (2022), 105411.
- [26] M. Zhou, A. Gallegos, K. Liu, S. Dai, J. Wu, Insights from machine learning of carbon electrodes for electric double layer capacitors, *Carbon* 157 (2020) 147–152.
- [27] M. Rahimi, M.H. Abbaspour-Fard, A. Rohani, Synergetic effect of N/O functional groups and microstructures of activated carbon on supercapacitor performance by machine learning, *J. Power Sources* 521 (2022), 230968.
- [28] P. Liu, Y. Wen, L. Huang, X. Zhu, R. Wu, S. Ai, T. Xue, Y. Ge, An emerging machine learning strategy for the assisted-design of high-performance supercapacitor

- materials by mining the relationship between capacitance and structural features of porous carbon, *J. Electroanal. Chem.* 899 (2021), 115684.
- [29] N. Elgrishi, K.J. Rountree, B.D. McCarthy, E.S. Rountree, T.T. Eisenhart, J. L. Dempsey, A Practical Beginner's Guide to Cyclic Voltammetry, *J. Chem. Educ.* 95 (2) (2018) 197–206.
- [30] M. Adil, R. Ullah, S. Noor, N. Gohar, Effect of number of neurons and layers in an artificial neural network for generalized concrete mix design, *Neural. Comput. Appl.* 34 (11) (2022) 8355–8363.
- [31] H.C. Yuan, F.L. Xiong, X.Y. Huai, A method for estimating the number of hidden neurons in feed-forward neural networks based on information entropy, *Comput. Electron. Agric.* 40 (1) (2003) 57–64.
- [32] M. Riedmiller, H. Braun, A direct adaptive method for faster backpropagation learning: the RPROP algorithm, in: *IEEE International Conference on Neural Networks*, 28 March-1 April 1993 1, 1993, pp. 586–591.
- [33] E. Pameté, F. Beguin, Effect of salt concentration in aqueous LiTFSI electrolytes on the performance of carbon-based electrochemical capacitors, *Electrochim. Acta* 389 (2021), 138687.
- [34] T. Lv, L. Suo, Water-in-salt widens the electrochemical stability window: Thermodynamic and kinetic factors, *Curr. Opin. Electrochem.* 29 (2021), 100818.
- [35] T. Zhang, B. Fuchs, M. Secchiaroli, M. Wohlfahrt-Mehrens, S. Dsoke, Electrochemical behavior and stability of a commercial activated carbon in various organic electrolyte combinations containing Li-salts, *Electrochim. Acta* 218 (2016) 163–173.
- [36] K. Xu, M.S. Ding, T. Richard Jow, A better quantification of electrochemical stability limits for electrolytes in double layer capacitors, *Electrochim. Acta* 46 (12) (2001) 1823–1827.
- [37] L. Coustan, K. Zaghib, D. Bélanger, New insight in the electrochemical behaviour of stainless steel electrode in water-in-salt electrolyte, *J. Power Sources* 399 (2018) 299–303.
- [38] A. Mistry, A.A. Franco, S.J. Cooper, S.A. Roberts, V. Viswanathan, How Machine Learning Will Revolutionize Electrochemical Sciences, *ACS Energy Lett.* 6 (4) (2021) 1422–1431.
- [39] J. Ren, X. Lin, J. Liu, T. Han, Z. Wang, H. Zhang, J. Li, Engineering early prediction of supercapacitors' cycle life using neural networks, *Mater. Today Energy* 18 (2020), 100537.
- [40] J. Wang, Z. Li, S. Yan, X. Yu, Y. Ma, L. Ma, Modifying the microstructure of algae-based active carbon and modelling supercapacitors using artificial neural networks, *RSC Adv.* 9 (26) (2019) 14797–14808.
- [41] F. Tavazza, B. DeCost, K. Choudhary, Uncertainty Prediction for Machine Learning Models of Material Properties, *ACS Omega* 6 (48) (2021) 32431–32440.